PROPERTIES OF INTERPLANETARY CORONAL MASS EJECTIONS

NAT GOPALSWAMY

NASA Goddard Space Flight Center, Greenbelt, MD 20771, USA
(E-mail: gopals@ssedmail.gsfc.nasa.gov)

Abstract. Interplanetary coronal mass ejections (ICMEs) originating from closed field regions on the Sun are the most energetic phenomenon in the heliosphere. They cause intense geomagnetic storms and drive fast mode shocks that accelerate charged particles. ICMEs are the interplanetary manifestations of CMEs typically remote-sensed by coronagraphs. This paper summarizes the observational properties of ICMEs with reference to the ordinary solar wind and the progenitor CMEs.

Keywords: coronal mass ejections, interplanetary CMEs, solar wind, magnetic clouds, shocks, solar flares, geomagnetic storms

1. Introduction

There are two classes of large-scale interplanetary (IP) structures related to the two types magnetic field topology on the Sun: interplanetary coronal mass ejections (ICMEs) originating from closed field regions and corotating interaction regions (CIRs) due to high speed streams originating from open field regions (see, e.g., Gosling, 1996, for a review). Two earlier ISSI volumes have extensively dealt with CIRs (Balogh *et al.*, 1999) and CMEs (Kunow *et al.*, 2006). Both CIRs and ICMEs are capable of driving shocks, which in turn, accelerate charged particles. The CIR shocks generally form far beyond 1 AU, although they are occasionally observed near 1 AU. ICME are the IP manifestations of CMEs. CMEs drive shocks from close to the Sun to far into the IP medium, the shocks being the strongest near the Sun. CME-driven shocks accelerate charged particles from close to the Sun and in the IP medium. ICMEs are responsible for the severest of geomagnetic storms when they impinge upon Earth's magnetosphere. ICMEs also provide an enormous plasma laboratory to study physical processes in space. The white light CMEs observed near the Sun are typically 10 times more abundant than the ICMEs observed *in situ* (Gopalswamy, 2004). ICMEs are therefore a special population that makes significant impact on the heliosphere, in particular on Earth's space environment. In fact Earth spends in the flows related to ICMEs anywhere from 10% of the time during solar minimum to 35% of the time during solar maximum (Cliver *et al.*, 2003). ICMEs are also observed throughout the heliosphere (see, e.g., Burlaga, 1995; Balogh, 2002).

Early ideas on transient plasma ejections from the Sun can be found in the reviews by Burlaga (1995) and Gosling (1997). The first IP shock was identified from the Mariner 2 plasma and magnetic field measurements (Sonnet *et al.*, 1964). Since solar flares were known for a much longer time, early studies focused on the connection between solar flares and IP shocks (see, e.g., Dryer, 1994, for a review). White-light CMEs were first detected by NASA's seventh Orbiting Solar Observatory (OSO-7) on December 14, 1971 (Tousey, 1973). Although the connection between coronal shocks (inferred from metric type II radio bursts) and IP shocks (detected *in situ* and inferred from IP type II bursts) was recognized early on (Pinter, 1973), the correspondence between CMEs and their IP counterparts (ICMEs) became clear when Helios 1 observed an ICME (June 20, 1980) that left the Sun two days before as a CME observed by the Solwind coronagraph on board P78-1 (Burlaga *et al.*, 1982).

Helios 1 detected a magnetic loop behind an IP shock, which Burlaga *et al.* (1981) defined as a magnetic cloud (MC), a name given to those ICMEs that have a high magnetic field, smooth field rotation, and low proton temperature (Lepping *et al.*, 1990). The term "magnetic cloud" was originally used by Parker (1957) in a much broader sense in his theoretical study of the dynamics of hydromagnetic gas clouds ejected from the Sun into the IP space. ICMEs are identified using plasma, magnetic, compositional and energetic particle signatures (see, e.g., Gosling *et al.*, 1990). These signatures include bidirectional streaming of superthermal electrons and ions, unusual abundances and charge states, low electron and proton temperatures, strong magnetic fields with flux rope structures, and Forbush decrease. It must be noted that not all of the signatures are present in all events (see Neugebauer and Goldstein, 1997). *In situ* observations can be used to infer the magnetic field topology of the ICMEs and the physical conditions of their birthplace near the Sun (see, e.g., Henke, 1998; Lepri *et al.*, 2001).

This paper summarizes the properties of ICMEs in relation to the white light CMEs. After an observational description of ICMEs in Section 2, their statistical properties are summarized in Section 3 in comparison with the solar wind. The solar origin of ICMEs, the source locations, and their variation with the solar activity cycle are discussed in Section 4. The charge state composition of ICMEs and its solar origin is discussed in Section 5. In Section 6, the connection between ICMEs and geomagnetic storms is discussed. Section 7 gives the summary and conclusions.

2. An Observational Description of ICMEs

ICMEs are transient disturbances in the solar wind referred to by various names such as driver gas, ejecta, and plasma cloud. ICMEs are recognized as large-scale magnetic structures with magnetic field enhanced with respect to the solar wind and having plasma and composition signatures distinct from the solar wind in which
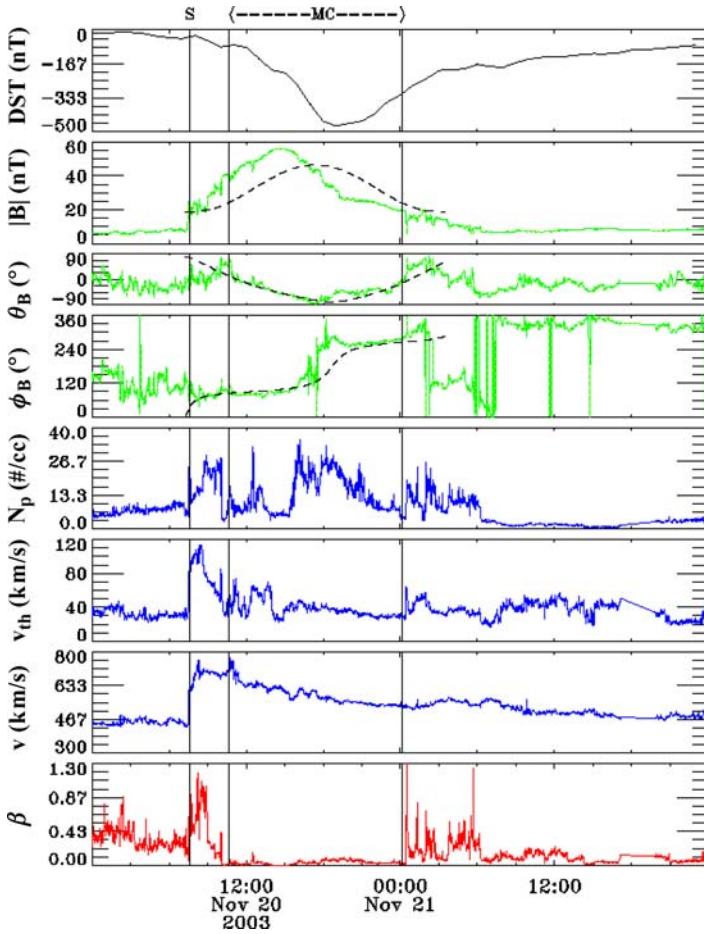
Figure 1. The magnetic cloud event of 2003 November 20 with the associated geomagnetic storm index (*Dst*), the magnetic field strength (|**B**|), the latitude (θ_B), longitude (ϕ_B) of the cloud, and the solar wind parameters (proton density N_p, proton thermal speed V_{th}, flow speed V and the plasma beta β). The dashed curves in the |**B**|, θ_B, and ϕ_B are model fits. The boundaries of the cloud (MC) and the shock (S) are marked at the top from Goplswamy *et al.* (2005a).

they are embedded. When the ICME has a flux rope structure, it is called an MC, as defined by Burlaga *et al.* (1981). Observations of an ICME (MC in this case) are shown in Figure 1. The MC interval is marked by the two vertical lines. The MC was driving a shock, which was located about 2.5 h ahead of the MC. The MC was associated with an intense geomagnetic storm (*Dst* = −472 nT) shown at the top (Gopalswamy *et al.*, 2005a). The magnetic field strength is very high, with the peak value of ∼ 56 nT. The polar and azimuthal angles of the magnetic field are also smooth during the cloud interval. The polar angle shows that the cloud is highly inclined to the ecliptic plane (–73.4 degrees) and south-pointing throughout
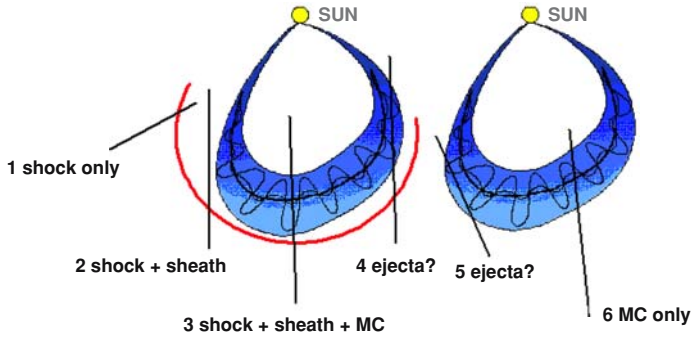
Figure 2. Six possible tracks of an observing spacecraft through an MC with a leading shock (left) and another without (right). Tracks 1 and 2 never encounter the MC proper. They pass through the shock and the compressed ambient medium in one of the flanks of the MC. Track 4 passes through the nose of the MC. This situation arises when the observing spacecraft is along the Sun-Earth line and a fast and wide CME erupts from close to the Sun center. Trajectory 4 passes through the shock, sheath, and through the edge of the MC. Tracks 5 and 6 are similar to 4 and 3, respectively, except that the MC is slow and hence it does not drive a shock. Trajectories 4 and 5 are not expected to observe an MC structure.

the cloud. In addition, the azimuthal angle shows a smooth rotation from east to west, so such clouds are called ESW cloud. The solar wind density is enhanced in the region between the cloud and the shock (a region known as the shock sheath). The proton thermal speed also has a jump in the sheath and is low in the cloud. The MC was expanding, evidenced by the smooth decrease in speed from the front (738 km/s) to the back (531 km/s), with an average value of 625 km/s. There was a slight increase in speed after the MC, probably due to a high speed stream originating from a coronal hole. The plasma β is extremely low during the cloud interval, showing the dominance of the magnetic field. The duration of the cloud is ∼14 h. Since the cloud was moving with an average speed of ∼625 km/s, this duration corresponds to a cloud thickness of ∼0.21 AU. This thickness is consistent with the cloud diameter inferred from multi-spacecraft observations. For example, Burlaga *et al.* (1990) used Helios 1, Helios 2, IMP-8 and Voyager-2 data ICMEs to infer a loop-like structure (see Figure 2) with a radius of curvature of ∼0.35 AU and a cloud diameter of 0.25 AU. They also inferred that the legs of the loop must be connected to the Sun at both ends.

As the observing spacecraft passes from the outer boundary of the loop structure in Figure 2 to the axis and then to the inner boundary, the azimuthal field changes sign at the axis, indicating the rotation of the field direction. The magnitude of the azimuthal component also changes, peaking at the axis and falling off on either side. The cloud can drive a shock if it is super-Alfvenic. The shock standoff distance corresponds to a lead time of ∼0.5 day. i.e., a spacecraft in the solar wind first encounters the shock and then the cloud several hours later. The trajectory of the

observing spacecraft essentially decides the observed structure. When the trajectory goes through the nose of the magnetic cloud (tracks 3 and 6), one observes an MC as in Figure 1. Tracks 4 and 5 will not observe a cloud structure because of the skimming trajectory. The extreme case is when the trajectory never passes through the cloud, but only through the shock sheath (track 2) or simply the shock (track 1). The "shock only" and "shock + sheath" configurations are readily observed. The interpretation of the general ejecta corresponding to tracks 4 and 5 is not clear. According the picture presented in Figure 2, all ICMEs have cloud structure, but the vantage point decides the appearance as an MC or ejecta. One of the other possible interpretations is that the ICME contains just untwisted loops ejected from active regions and hence do not show any MC structure (Gosling, 1990). It is really an open question whether all the ICMEs have flux rope structures.

3. Statistical Properties

3.1. SOLAR WIND PROPERTIES

To see the ICME as disturbances superposed on the solar wind, we first show the distributions of magnetic field strength, speed, density and temperature of the solar wind obtained from Omniweb for a time period 1996–2003 (see Figure 3). Note that the solar wind parameters obtained from Omniweb correspond to a heliocentric distance of 1 AU and may have different values at other distances. The number of hours with missing data was only a small fraction (<8%). The distributions with and without ICMEs are similar because the duration over which Earth was immersed in CME-related solar wind is only ~28% on the average. When the ICME intervals (see, e.g., Cane and Richardson, 2003; Lepping *et al.*, 2005) are removed, the solar wind magnetic field and speed show slightly lower values, the density did not show much change and the temperature was slightly higher. This is consistent with the general property that ICMEs have enhanced magnetic field and reduced temperature.

3.2. PROPERTIES OF ICMES

To get the properties of ICMEs, we need an accurate list. The identification of ICMEs, especially their boundaries, has been highly subjective and controversial (see, e.g., Russell and Shinde, 2005 and references therein), but the overall numbers obtained by various authors is similar. Here we use the following subsets of ICMEs: MCs identified manually using the Burlaga criteria, the cloud-like events identified by automatic detection (Lepping *et al.*, 2005), and ICMEs following IP shocks (Manoharan *et al.*, 2004). The automatic detection of cloud-like events employed the following criteria (Lepping *et al.*, 2005): (1) low plasma beta (≤0.3),
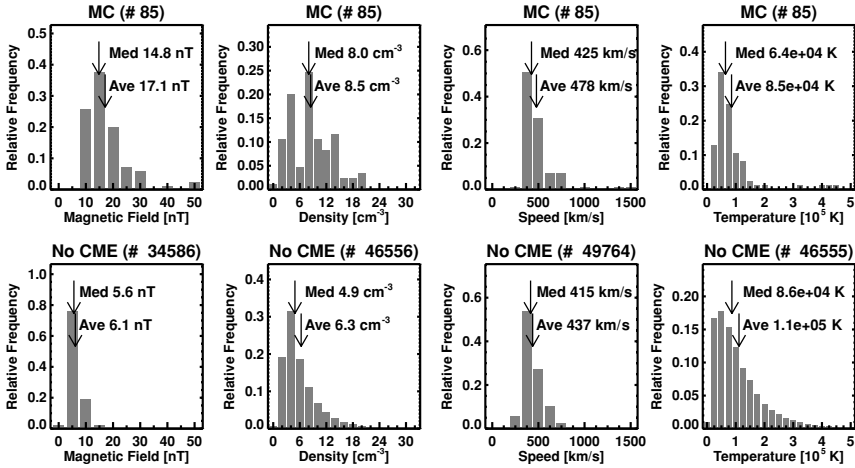
Figure 3. Distributions of magnetic field strength, density, speed, and temperature of the solar wind over the interval 1996–2003 (inclusive) with (top) and without (bottom) ICMEs. Data from Omniweb (http://omniweb.gsfc.nasa.gov) with one-hour time resolution were used. The number of data points (i.e., the number of hours) is indicated at the top. The total number of hours during the study interval is 70128, which means a relatively small data gaps for magnetic field (1.7%), density (7.8%), speed (2.2%), and temperature (7.8%). The mean and median values of the distributions are marked. The plots excluding ICMEs ("No CME") were created by removing the data points corresponding to ICME intervals.

(2) magnetic field with slowly changing direction, (3) enhanced magnetic field over an interval of ≥ 8 h, (4) average magnetic field ≥ 8 nT, (5) low proton thermal speed (≤ 30 km/s), and (6) large latitudinal difference angle (≥ 45 deg). Lepping *et al.* (2005) could identify most of the MCs also by this method. From the list generated by automatic detection, the manually identified MCs were eliminated to get the list of cloud-like events. Figure 4 summarizes the properties of MCs, cloud-like events, and shock-driving ICMEs. The maximum magnetic field strength in the three populations of ICMEs ranged from a few nT to several tens of nT, generally much larger than the average solar wind value (6.1 nT, see Figure 3). The mean speeds of MCs (478 km/s) and shock-driving ICMEs (484 km/s) were generally larger than those of the cloud-like events (412 km/s) and the slow solar wind (437 km/s). During the occasional extreme events, MCs had speeds exceeding 1000 km/s. Overall, MCs and shock-driving ICMEs have higher maximum field strength, speed, and duration compared to the cloud-like events. The proton thermal speed of the cloud-like events was higher than that of the MCs but lower than that of the shock-driving ICMEs.

Figure 5 shows the scatter plots between maximum magnetic field strength and speed of ICMEs measured *in situ*. There is certainly a weak correlation between the maximum field strength and speed for the MCs, but there is no such correlation for the cloud-like events. The shock-driving ICMEs, on the other hand, have a
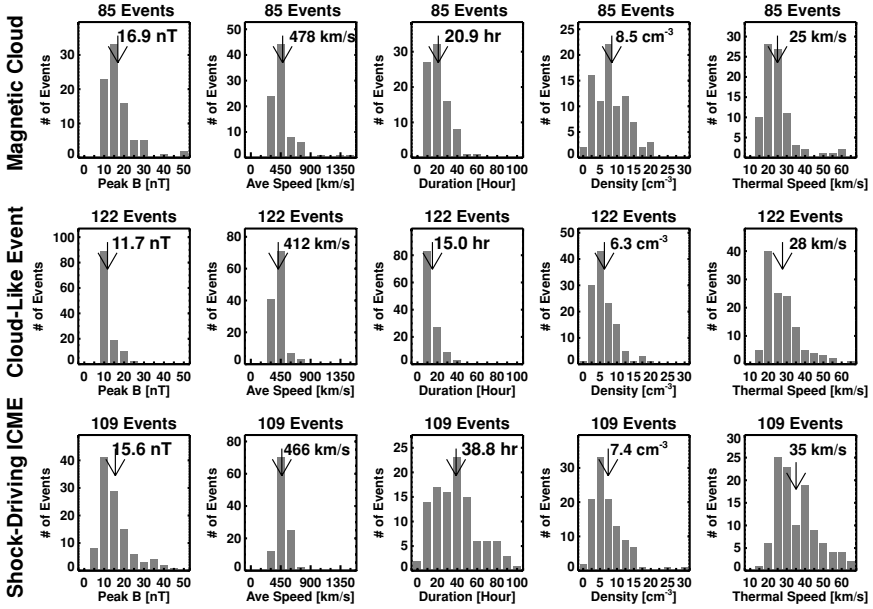
Figure 4. Properties of ICMEs grouped into magnetic cloud (top), cloud-like (middle) events, and shock driving ICMEs (bottom) that are not MCs. Distributions of the magnetic field strength, speed, duration, density, and thermal speed within the cloud are shown. The magnetic field strength is the peak value within the ICME interval while all others are average values within the same interval. The averages of the distributions are indicated on the plots. The cloud-like events were identified using an automatic program. The sharp cutoffs of some of the distributions at the low end are due to the selection criteria employed by the automatic feature recognition routine.
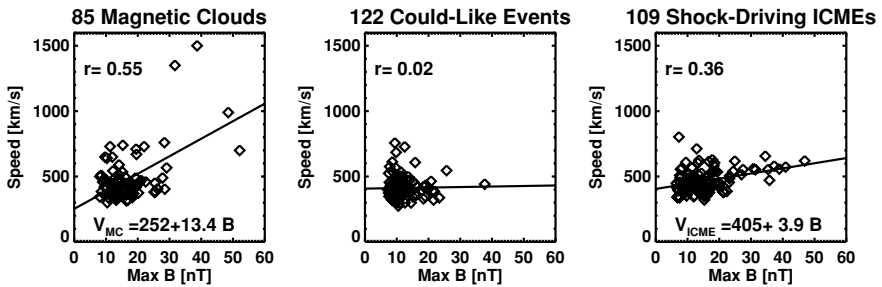

Figure 5. Correlation between the speed and magnetic field strength of MCs (left), cloud-like events (middle) and shock-driving ICMEs (right). The correlation coefficient (r) is marked in each case.

correlation much weaker than that for the MC events, but definitely positive compared to the cloud-like events. Gonzalez *et al.* (1998) had found a better correlation ($r = 0.75$) using a sample of 30 MCs. A bigger sample of 85 MCs (see Figure 5) yields a correlation coefficient of only 0.55. It must be pointed out that the MCs in Figure 5 have a wider range of speeds (300 to 1500 km/s) compared to that

in Gonzalez *et al.* (1998) (350 to 750 km/s). The corresponding regression lines are: $V_{MC} = 23.4 + 21.28 B_{MC}$ from Gonzalez *et al.* (1998) compared to MC speed $V_{MC} = 252 + 13.4$ magnetic field B_{MC} for the 85 MCs in Figure 5 (V_{MC} in km/s and B_{MC} in nT). Gonzalez *et al.* (1998) suggested that the poor correlation between speed and magnetic field strength in non-MC driver gas may be due to the geometrical effect that the observing spacecraft does not pass through the center of the cloud and hence measures lower field strength (corresponding to tracks 4 and 5 in Figure 2).

3.3. ICMEs AND SHOCKS

Interplanetary shocks are important players in Sun-Earth connection because they accelerate energetic particles near the Sun and when they arrive at 1 AU (energetic storm particle events, see Rao *et al.*, 1967), mark the sudden commencement of magnetic storms (Chao and Lepping, 1974), and signal the impending arrival of ICMEs. Most of the IP shocks observed within 1 AU can be identified with ICMEs. Occasionally, shocks driven by CIRs are observed, but these generally form beyond 1 AU (see, e.g., Burlaga *et al.*, 1995). Lindsay *et al.* (1994) surveyed IP shocks within 0.72 AU from the Sun and found that most of them (80%) were associated with ICMEs (the other 20% being CIR-driven). However, starting from MCs, Klein and Burlaga (1982) found that only a third of them were preceded by IP shocks. Much higher rate of association was also reported in two later studies (70% by Marsden *et al.*, 1987 and 80% by Zhang and Burlaga, 1988). Gopalswamy *et al.* (2000) found that 25 of the 28 ICMEs (89%) during the period 1996–1998 were driving shocks. They found similar results (92–93% association) for an expanded data set (Gopalswamy *et al.*, 2001a). The number of shocks varies in phase with the solar activity cycle (Lindsay *et al.*, 1994). Since the shocks need faster and wider CMEs to drive them the solar-cycle variation of the number of shocks actually tracks the fast and wide CMEs better (Gopalswamy *et al.*, 2003). Figure 6 shows a scatter plot between the shock and MC speeds. The correlation coefficient is $r = 0.95$. Such a tight relationship suggests that the shocks are driven even at 1 AU (Gopalswamy *et al.*, 2005b). Occasionally, shocks are observed at 1 AU, which do not seem to have a driver behind them. However, this is due to an observation limitation: the spacecraft passes through the shock, but not through the driver as illustrated in Figure 2 (tracks 1 and 2). In these cases, the associated CME at the Sun is ejected roughly at right angles to the Sun-Earth line.

4. The Solar Connection

The close connection between CMEs and ICMEs was recognized in 1982 when a Helios-1 MC was identified with a white-light CME that left the Sun two days before (Burlaga *et al.*, 1982). The high speed plasmas with helium abundance
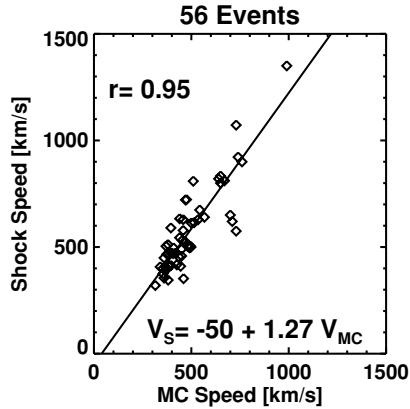
Figure 6. Scatter plot between MC speeds (V_{MC}) and the speeds of the associated shocks (V_S) for the period 1996–2003 from Gopalswamy *et al.* (2006).

enhancement behind IP shocks was recognized as the IP counterparts of CMEs (Borrini *et al.*, 1982). Howard *et al.* (1982) identified a halo CME observed by the Solwind coronagraph with an IP shock observed by ISEE-3 three days later at 1 AU. Sheeley *et al.* (1985) used quadrature observations to show that most of the IP shocks had associated white light CMEs. They also found that nearly half of these IP shocks had driver gas (ICME) behind them. Magnetic clouds have also been found to be related to prominence eruptions (e.g. Burlaga *et al.*, 1982; Wilson and Hildner, 1986; Marubashi, 1986; Bothmer and Schwenn, 1994; Rust, 1999) and flares (see, e.g., Bravo *et al.*, 1998). However, prominence eruptions form the inner core of white-light CMEs (Hori and Culhane, 2002; Gopalswamy *et al.*, 2003b) and eruptive flares are indicative of CMEs (Munro *et al.*, 1979). Thus these surface eruptive signatures are proxies to CMEs. With the simultaneous availability of white light images of CMEs and *in situ* observations, it has become possible to routinely identify the CME corresponding to each ICME. Similarly, when bright halo CMEs appear from close to the disk center, they are highly likely to result in an ICME 1–4 days later.

Unfortunately, there is no simple way to continuously observe CMEs evolving into ICMEs at present. The situation will change soon since the STEREO mission has been launched. Tracking type II radio bursts from the corona into the IP medium is one way of tracking the shocks ahead of CMEs, but not the CMEs. Interplanetary scintillation observations is another possible way, but what is tracked may not be the CME proper, but the disturbed region in the front (see, e.g., Manoharan *et al.*, 2006). MHD modeling can also bridge the gap between coronal and solar wind observations (see, e.g., Roussev and Sokolov, 2006). As the standoff distance of the shock from the CME corresponds to a separation of ∼0.5 day, it is important to identify the substructures of an ICME for a proper understanding of the CME-ICME relationship. Gopalswamy (2003) proposed the following scenario

for the relation between CMEs and ICMEs. Shocks in the corona associated with white light CMEs are well established, so associating them with the leading shocks in ICMEs is straightforward. The sheath behind ICMEs can be associated with the bright front of CMEs. There are some difficulties with this regarding the topology of the field lines in the sheath (closed or open). The magnetic cloud structure in ICMEs can be thought of as the evolved form of the coronal cavity seen as dark void in coronagraphic images. Recent observations clearly show the existence of flux rope structure in the void region (see, e.g., Chen *et al.*, 1997). Finally, as we noted above, the eruptive prominences are the slowest and most sunward feature of CMEs. Such features are rarely observed inside ICMEs, but occasionally show up at the bottom of MCs as cool material (Burlaga *et al.*, 1998; Gopalswamy *et al.*, 1998). Post-flare loops and arcades observed in H-alpha, X-ray and EUV are features anchored to the Sun and are indicative of a CME eruption. Thus it is possible that the four-part structure (shock, sheath, flux rope, and prominence) is maintained throughout the inner heliosphere. Of course one or more of the substructures may not be present in all CMEs. For example, if the CME is sub-Alfvenic, it will not drive a fast-mode shock.

4.1. CME ACCELERATION

While most of the early works concentrated on relating white-light CMEs to IP shocks, recent studies have focused on the connection between white light CMEs and ICMEs (Lindsay *et al.*, 1999; Gopalswamy *et al.*, 2000, 2001b, 2005b; Schwenn *et al.*, 2005). Lindsay *et al.* (1999) found a linear relation between CME and ICME speeds and confirmed that slow CMEs accelerate and fast CMEs decelerate as a result of interaction with the solar wind. Gopalswamy *et al.* (2000) quantified this acceleration using SOHO and Wind observations and improved it further using quadrature data from Solwind coronagraph and Pioneer Venus Orbiter (PVO) data (Gopalswamy *et al.*, 2001b). The interplanetary acceleration a (m/s^2) was found to be related to the CME speed V (km/s) in the corona as $a = -0.0054(V - 406)$. Thus CMEs with $V < 406$ km/s accelerate, while those with $V > 406$ km/s decelerate. CMEs have constant speed when $V = 406$ km/s. The critical speed of 406 km/s was identified with the solar wind speed. Figure 7 shows the effect of this IP acceleration for a set of 59 CME-MC pairs. These MCs form a subset of those in Figure 2 for which the corresponding white light CMEs were identified. Note that the white light CMEs have a much wider distribution of speeds than the MCs. The average MC speed is also considerably lower than the average white light CME speed. The IP acceleration was found to be the same whether they are MCs or ejecta. Figure 7 also shows that CMEs resulting in MCs are much faster than the solar wind on the average.

The acceleration can be used to determine the ICME speed and arrival time based on the white light CME speed. Figure 8 (left) shows a scatter plot of observed
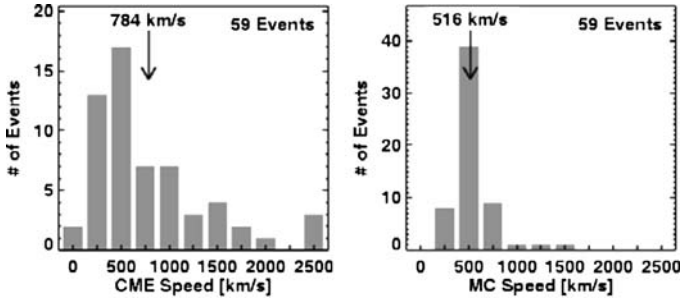
Figure 7. The speed distribution of CMEs (left) and ICMEs (right) for a set of 59 CME-ICME pairs. This is an updated version of the original figure in Gopalswamy *et al.* (2000).
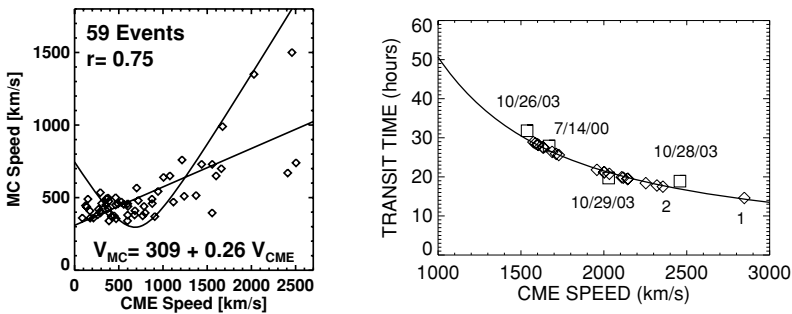

Figure 8. (left) CME and MC speeds for the 59 CME-MC pairs. The straight line is Lindsay *et al.* (1999) formula. The parabolic curve is from Gopalswamy *et al.* (2001b). (right) the empirical shock arrival model for (solid curve) with some very fast events (diamonds) including the Carrington events of 1859 September 1 (marked 1) and August 4, 1972 (marked 2). The squares are actual measurements of CME speeds from SOHO and the observed shock transit times.

MC and white light CME speeds, along with the final-speed curves according to Lindsay *et al.* (1999) and Gopalswamy *et al.* (2001b). The regression line ($V_{MC} = 309 + 0.26V_{CME}$) in Figure 8 is almost the same as the one obtained by Lindsay *et al.* ($V_{MC} = 360 + 0.25V_{CME}$). White light CMEs have been observed to have speeds exceeding 2500 km/s. For these CMEs, Lindsay *et al.* (1999) formula gives a final speed of only ∼985 km/s. During the October November 2003 period, one ICME exceeded a speed of ∼1500 km/s, while the progenitor CME had a speed of ∼2500 km/s (Gopalswamy *et al.*, 2005c). For such high speed ICMEs, the parabolic curve suits better. It must be pointed out that the IP acceleration was obtained from quadrature observations, so the projection effects are minimal. The CME speeds used in Figure 8 are in the plane of the sky. Using space speeds should yield a better comparison. The IP acceleration can also be used to estimate the arrival time of ICMEs based on the speed and onset time at the Sun. The tight relationship between IP shocks and the driving ICMEs shown in Figure 6 has been used to extend the CME arrival model to shock arrival model shown in Figure 8 (right).
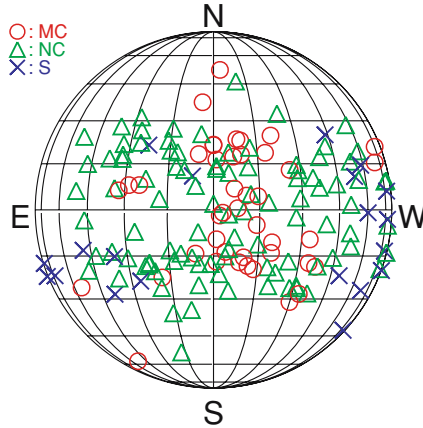
Figure 9. The solar source locations of CMEs associated with MCs (circles) and non-cloud ICMEs (NC – triangles) for the period 1996–2002 (inclusive). The non-cloud ICMEs were all driving shocks. The crosses indicate shocks (S) which have their driving CMEs propagating orthogonal to the Sun-Earth line, so the driver is not encountered by the observing spacecraft located along the Sun-Earth line. Note that the magnetic clouds generally originate from close to the disk center, shocks without drivers are due CMEs originating from close to the limb. The events were chosen based on the detection of *in situ* shocks at 1 AU.

Schwenn *et al.* (2005) have suggested a way to avoid the projection effects. They find that the radial speed (V_{rad}) is related to the expansion speed (V_{exp}) in the sky plane according to: $V_{rad} = 0.88 V_{exp}$.

Propagation of CMEs can also be affected by interaction with other CMEs (Gopalswamy *et al.*, 2001c) near the Sun (Manoharan *et al.*, 2004) and in the IP medium (Burlaga, 1995; Burlaga *et al.*, 2002). It was shown that the Sun-Earth transit time of ICMEs interacting with preceding CMEs is generally larger than those of isolated CMEs. At 1 AU, complex ejecta have been observed when successive CMEs interact and produce extended structures at 1AU, whose thickness may fill the entire Sun-Earth space.

4.2. SOLAR SOURCES

Figure 9 shows the solar sources of CMEs associated with MCs, shocks, and non-cloud ICMEs. The identification of non-cloud ICMEs is different from the CLs used above although there is significant overlap. The non-cloud ICMEs were compiled by starting with a list of IP shocks detected *in situ*, identifying the driver behind them (see Manoharan *et al.*, 2004), and eliminating known MCs from the list. The selection criterion excludes those non-cloud ICMEs that do not drive a shock, resulting in a slight underestimation of the number of non-cloud ICMEs. As for the MCs, we have included all the events that had corresponding white-light CMEs. The solar sources were identified from the location of the associated flare, filament
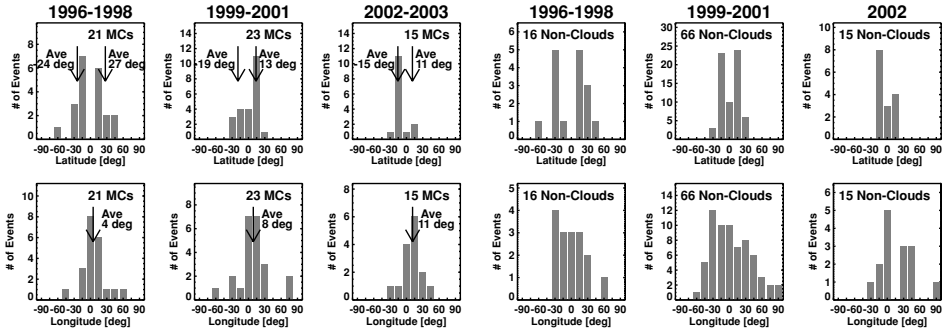
Figure 10. Latitude and longitude distributions of solar sources of MCs (left) and non-cloud events (right) for three phases of the solar cycle: minimum to rise phase (1996–1998), maximum phase (1999–2001) and the declining phase (2002–2003). Data from Gopalswamy *et al.* (2006).

eruption, post eruption arcades (X-rays and EUV), or EUV dimming signature. The non-cloud events also include a few shocks with no associated ICMEs, but did have associated white-light CMEs. These CMEs are heading in a direction predominantly orthogonal to the Sun-Earth line, so the ICMEs are not encountered by the observing spacecraft. One can see the following pattern in the source location of CMEs associated with IP events: (i) CMEs associated with MCs occur very close to the disk center with a slight westward bias, (ii) CMEs associated with non-cloud ejecta are scattered over a wide range of longitudes and have intermediate central meridian distances, and (iii) CMEs associated with just IP shocks (no driver gas) occur at large central median distances. Such a pattern supports the idea that all ICMEs are MCs, but the trajectory of the observing spacecraft can make an MC appear as ejecta without flux-rope structure, as illustrated in Figure 2. It must be pointed out that there are quite a few non-cloud MCs that originate close to the disk center. It is not clear whether these ICMEs have an inherent non-cloud structure (Gosling *et al.*, 1990) or they have cloud structure but the propagation results in sampling of the flux rope edges.

4.3. SOLAR CYCLE VARIATION OF CME LATITUDES

The latitude and longitude distributions of the MC and non-cloud events are shown grouped into three phases of the solar activity cycle in Figure 10: the minimum phase (1996–1998), the maximum phase (1999–2001) and the declining phase (2002–2003). The longitude distributions generally peak close to the central meridian during all the three phases. The latitudinal distribution is dramatically different during different phases. During 1996–1998, the latitude distribution has a clear bimodal structure, corresponding to the active region belt in the north and south. The MCs originated predominantly in the northern hemisphere during the maximum phase, and in the southern hemisphere during the declining phase (2002–2003). It

is not clear if this is due to the level of activity in the hemisphere or the global field has some influence. During the minimum phase, there is certainly the influence of the global solar dipole field which tends to move CMEs originating from higher latitudes towards the equatorial plane. This may be one of the reasons for a higher abundance of the MCs during the minimum phase and an under-abundance during the maximum phase, while the total number of ICMEs had a solar cycle variation similar to that of the general population of white light CMEs (see Wu *et al.*, 2006; Riley *et al.*, 2006).

It is well known that MCs originating from the northern (southern) hemisphere of the Sun have negative (positive) chirality (Bothmer and Schwenn, 1994). This pattern generally matches with the active region helicity and filament chirality (see, e.g., Pevtsov *et al.*, 2001). Since CMEs are expected to remove the accumulated helicity in the corona (see, e.g., Low, 1996), the hemispheric dependence of occurrence rate is expected to result in a preferred chirality of the MCs.

The latitude and longitude distributions of the non-cloud ICMEs have roughly the same solar cycle variation as the MCs, but less pronounced. One important difference is the number and distribution of non-cloud ICMEs during the maximum phase: the longitude distribution is much wider and shows pronounced western bias. The number of non-cloud events during the maximum phase is about 3 times larger than the number of MCs during the same phase. One possibility is that during solar maximum there is a large number of CMEs, but they are not channeled towards the equator (due to the weaker dipole field).

5. Composition Signatures

The charge state distributions of heavy ions observed in the interplanetary plasmas reflect the conditions in the coronal environment where the plasmas originate. This applies to both the ordinary solar wind and the ICMEs. The charge state composition can often distinguish the fast wind from slow wind (von Steiger and Zurbuchen, 2003) because they originate from different coronal regions (fast wind from coronal holes and slow wind from streamers). In fact the difference in charge state distributions is one of the important ways of identifying ICMEs against the background solar wind (see, e.g., Galvin, 1997; von Steiger *et al.*, 1995). Since the time scale for solar wind expansion is typically much shorter than that of ionization and recombination, the relative ionization states get frozen, maintaining the source values (Hundhausen *et al.*, 1968). Thus high ionization states are indicative of a hot source region, and one can construct the thermal history of the interplanetary plasmas by comparing the freezing-in temperatures of different charge state pairs.

5.1. HIGH CHARGE STATES

Henke *et al.* (1998, 2001) studied the compositional signatures of more than 50 ICMEs observed by Ulysses and found that the O^{7+}/O^{6+} ratio was significantly
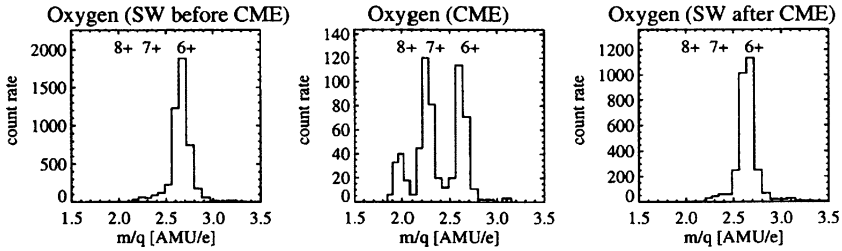
Figure 11. Ulysses observations of Oxygen charge states before, during, and after an ICME from Henke *et al.* (2001).

higher inside magnetic clouds (Xn + denotes the number density of atoms of an element *X* ionized n times). The correlation between the magnetic cloud structure and enhanced O^{7+}/O^{6+} ratio was confirmed for a much larger sample of ICMEs from the ecliptic (Aguilar-Rodriguez *et al.*, 2006). They found that the O^{7+}/O^{6+} and Mg^{10+}/O^{6+} ratios in magnetic clouds show a clear increase with respect to the ambient solar wind, whereas non-cloud ICMEs do not show such an increase. However, all types of ICMEs (MCs, non-cloud ejecta or complex ejecta) generally have a higher ionization states suggesting that ICMEs do originate from hot regions near the Sun. Figure 11 illustrates the dramatic increase in O^{7+} and O^{8+} ions within an ICME compared to the solar wind before and after the passage of the ICME. Similar effects could be seen in the charge state composition of other heavy elements such as Fe. In fact, Henke *et al.* (2001) found that almost all events with enhanced O^{7+}/O^{6+} ratio displayed an enhancement of the Fe^{12+}/Fe^{11+} ratio as well. Lepri *et al.* (2001) found that more than 90% of long-duration enhancements in Fe charge state in the solar wind were associated with ICMEs. However, the enhancements only occur in ~50% of ICMEs during 1998–2000. This again may be related to the requirement of magnetic cloud structure in ICMEs. Figure 12 shows a magnetic cloud event with distinct enhancement of O^{7+}/O^{6+} ratio and high Fe charge states only during the magnetic cloud interval. The magnetic cloud was driving a shock, but the sheath region has no charge state enhancement.

Reinard (2005) found that both O^{7+}/O^{6+} and Fe charge state (Q_{Fe}) are more likely to be enhanced for CMEs associated flares occurring close to the disk center. For a set of 67 ICMEs she studied, the average O^{7+}/O^{6+} ratio was 0.94, compared to the solar wind value (0.33) reported by Henke *et al.* (2001). When the central meridian events alone were considered, the average O^{7+}/O^{6+} ratio increased to 1.10. On the other hand, the average value for CMEs originating outside the disk-center region was only 0.45, close to the solar wind value. The average Q_{Fe} showed a similar behavior: the average values for central and non-central events were 12.7 and 10.5, respectively. The non-central value is very close to the solar wind values (10) obtained by Lepri and Zurbuchen (2004). It is well known that the CME plasma is observed at Earth only when the solar source is close to the disk center, typically within a central meridian distance of 30° (see, e.g., Gopalswamy *et al.*,
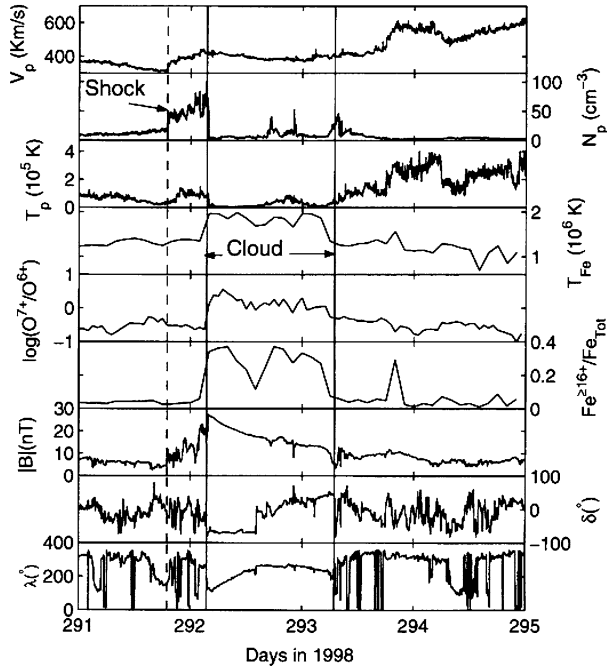
Figure 12. Enhancement of Fe charge state (Fe$^{\geq 16}$/Fe$_{tot}$), and O^{7+}/O^{6+} ratios at the time of a magnetic cloud during 1998 October 18–21. Also plotted are the proton velocity (V_p), density (N_p), temperature (T_p), Fe freeze-in temperature (T_{Fe}), magnetic field strength, latitude (δ), and longitude (λ). Note that the charge state enhancement occurs only during the MC interval. The Fe charge state enhancement is defined as the density ions with charge states Fe^{16+} and above relative to the density of all Fe ions from Lepri *et al.* (2001).

2000; Bravo and Blanco-Cano, 1998). This may be taken to indicate that only a spacecraft crossing along the center of the ICME will intersect the enhanced charge state ratios. Reinard (2005) also found a moderate correlation between flare size and the charge state ratio, further suggesting that flare heated material is trapped in the magnetic cloud structure.

5.2. LOW CHARGE STATES

Magnetic clouds occasionally contain low charge states (Zwickl *et al.*, 1982; Galvin, 1997; Burlaga *et al.*, 1998; Gopalswamy *et al.*, 1998). Fe, O, and C charge states down to 5+, 2+, and 4+ , respectively were reported by Zwickl *et al.* (1982), but these events are extremely rare. Such low charge states are indicative of cool material. The inner cores of CMEs contain eruptive prominence, which is the coolest component (∼8000 K) of the CME plasma at least initially. Gopalswamy *et al.* (1998) reported Fe charge states ranging from 5 to 11 in structures associated with the 1997 February 9 ICME. Towards the end of the ICME interval, a cold (proton

thermal speed <20 km/s and dense (proton density ~40 cm^{-3}) solar wind was observed by the WIND/MASS instrument. The presence of the low Fe^{5+} and Fe^{6+} in relatively high abundance ratio indicated that this plasma had originated from a relatively cold region in the corona, viz. the prominence. There were two other weaker pulses prior to the largest one and they are consistent with other prominence fragments ejected from under the same CME envelope.

5.3. CONNECTION TO FLARES

It has been shown that only $\sim10\%$ of CMEs observed near the Sun are detected in the heliosphere, irrespective of their latitude of origin (Gopalswamy, 2004). These CMEs are generally faster and wider on the average and hence more energetic. There is also a reasonable correlation between the CME kinetic energy and the X-ray flare size (see, e.g., Hundhausen, 1997). Therefore, one can see that ICMEs observed in the heliosphere are generally associated with large flares. Such flares are eruptive in nature, meaning they are associated with mass motion or CMEs. Flare sites are the only locations in the solar atmosphere were temperatures exceeding 10 MK are observed. The flare sites are connected to the CMEs so one can expect hot plasmas within CMEs. In the standard model of eruptive events (the so-called CSHKP model), the reconnection beneath the prominence causes injection of the prominence and hot plasma into the CME flux rope. The prominence structure is typically much smaller than the overall CME volume, which may be the reason for the rare occurrence of the prominence-related solar wind at 1 AU.

The correlation between O^{7+}/O^{6+} and the flare size reported by Reinard (2005) can easily be explained by the CSHKP model. The high charge states require a plasma near the Sun, hotter than the quiet corona. Flare plasma can have temperatures exceeding 10 MK. However, there is a small problem: the temperature of the flare material inferred from the charge state ratios (both O^{7+}/O^{6+} and Q_{Fe}) is much lower (<6 MK) than the flare temperature (>10 MK) inferred from soft X-ray observations. One possible reason is that the hot plasma entering the MC from the reconnection region (see Figure 12) might cool due to the expansion of the MC before reaching a height of $\sim4R_s$ where freezing in takes place. Another point to note is that the flare temperature is determined by the hot plasma detected in soft X-rays. This plasma is likely to have formed due to chromospheric evaporation due to energetic electron bombardment from the reconnection region. Similar situation does not exist in the upward direction.

One other place where higher temperature might exist is the shock down stream region (between the shock and the CME). However, no charge state enhancement if found in this region, again confirming the requirement of the magnetic topology. How about ICMEs originating close to the disk center, but not having magnetic cloud structure? These also seem to have enhanced charge state ratio. It is possible that these ICMEs also have MC structure, but the single point observation some how does not reveal it.
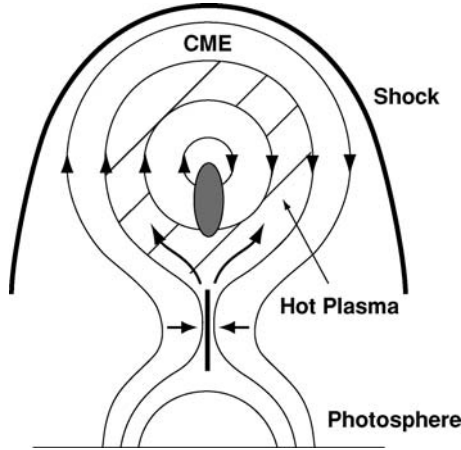
Figure 13. Model of a solar eruption adapted from Martens and Kuin (1989). The reconnection takes place at the current sheets (small vertical line above the closed field lines). The hot plasma trapped in the CME structure is indicated by the hashed region. The gray ellipse represents the prominence material. The solid curve at the top is the bow shock driven by the CME. The closed field region above the prominence is supposed to become the flux rope in the IP medium, to appear as in Figure 2.

6. ICMEs and Geomagnetic Storms

It has been established that ICMEs are the main source of major ($Dst < -100$ nT) geomagnetic storms (Gosling *et al.*, 1991; Bothmer and Schwenn, 1998; Tsurutani and Gonzalez, 1997; Webb *et al.*, 2000, 2002; Zhang *et al.*, 2003; Srivastava and Venkatakrishnan, 2004). CMEs on the Sun are intrinsically magnetic entities with large magnetic field strengths; they also compress any IMF at their leading regions when they travel through the interplanetary (IP) medium and interact with other IP CMEs (ICMEs) and/or the ambient solar wind driving IP shocks. Southward magnetic field (Bs) in shock sheaths and ICMEs contribute to the generation of the geomagnetic storms. As we noted before, the CMEs have to originate close to the disk center of the Sun to arrive at Earth before causing geomagnetic storms. Most of such CMEs are observed as halo CMEs. In fact, the properties of halo CMEs and geoeffective CMEs are nearly identical (Gopalswamy, 2006). This is because most of the front-side halos cause geomagnetic storms. While after-the-fact analysis shows the close connection between halo CMEs and geomagnetic storms, we are still far from predicting the occurrence and intensity of geomagnetic storms based on halo CME observations.

In order to illustrate the effect of the source location of CMEs on their geoeffectiveness, we consider a set of white-light CMEs from active region 0486 and the associated geomagnetic storms (see Figure 14). The first two CMEs originated from close to the disk center (and hence appear as full halos) and resulted in intense geomagnetic storms (–363 and –401 nT). The corresponding ICMEs were
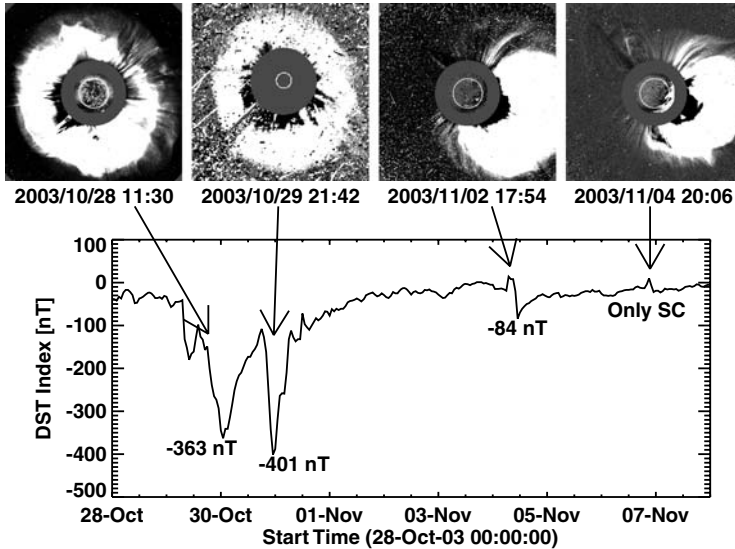
Figure 14. (top) Large CMEs from active region 0486 during October–November 2003 observed by SOHO/LASCO. The first two are symmetric full halos because the CMEs originated from close to the disk center. The last two CMEs occurred when the active region was close to the west limb, so they appear as partial halos. (bottom) A plot of the Dst index for the interval 2003 October 28 to November 7. The CMEs responsible for significant Dst events are shown by arrows from Gopalswamy *et al.* (2005c).

preceded by shocks and had magnetic cloud structure. On the other hand, the third CME is clearly a glancing blow to Earth as it is heading in the southwest direction. The CME was an asymmetric halo and only the eastern flank of the CME and the shock were encountered by Earth. The resulting geomagnetic storm had a sudden commencement due to shock impact followed by a weak storm due to the sheath. The last CME originated very close to the west limb and is unlikely to be encountered by Earth. The CME was one of the fastest of the cycle and was driving shock, yet the only thing happened was a sudden commencement. The first two CMEs correspond to track 3 in Figure 2 for a spacecraft along the Sun-Earth line. The second CME corresponds to track 2 while the last CME corresponds to track 1. Thus both the geoimpact and the identification of the ICME as an MC depend on the source location of the corresponding CME at the Sun.

An isolated magnetic storm typically lasts for ~1 day with a main phase of 3–12 hours and a recovery phase of ~14 hours (e.g., Tsurutani and Gonzalez, 1997). But geomagnetic storms are often complex, with a multiple-step decrease in Dst. These storms often have a longer duration and higher intensity. These complex geomagnetic storms (CGS) are sometimes referred to as multi-step storms or long-lived geomagnetic storms (LLGMS). High-speed streams (HSS) in corotating interaction regions (CIRs) cause only moderate to weak storms ($Dst > -100$ nT). CMEs on the Sun are intrinsically magnetic entities with large magnetic field strengths;

they also compress any IMF at their leading regions when they travel through the interplanetary (IP) medium and interact with other IP CMEs (ICMEs) and/or the ambient solar wind driving IP shocks. Southward magnetic field (Bs) in shock sheaths and ICMEs or magnetic clouds (MCs) contribute to the generation of the geomagnetic storms. While typical MCs have a south-to-north or a north-to-south structure, which ensures that the MCs are geoeffective either at the front or back, some MCs have high inclinations (see Mulligan *et al.*, 2001). The example given in Figure 1 has an axial field which is fully southward and produced the largest geomagnetic storm of cycle 23. In the opposite case of northward axial field, the MC is not geoeffective at all (Yurchyshyn *et al.*, 2001).

Burlaga *et al.* (2002) studied a set of fast ejecta observed at 1 AU from February 5, 1998 to November 29, 1999 and found that all MC events and two complex ejecta resulting from the interaction of multiple CMEs, produced geomagnetic storms. When HSS encounter and interact with CMEs, they can further compress Bz and enhance geoeffectiveness (e.g., Burlaga *et al.*, 1987; Burlaga, 1995; Gopalswamy *et al.*, 2005a). Thus, there are many sources of complexity in the IP medium, a systematic investigation of which will provide refinement to the existing knowledge on geoeffective solar events. Recently, Xie *et al.* (2006) studied a set of 37 complex storms with $Dst < -100$ nT and identified the associated white light CMEs. They found that $\sim$65% of such storms are caused by successive CMEs. They also found that $\sim$22% of the complex storms were caused by isolated CMEs while CIRs accounted for $\sim$13%. The storm duration is well correlated with the number of participating CMEs (correlation coefficient $r = 0.78$). This study also found that more intense storms resulted when there is interaction among CMEs and/or with HSS events.

7. Summary

Interplanetary coronal mass ejections represent the most energetic events in the heliosphere originating from the closed field regions on the Sun. White-light CMEs observed by coronagraphs evolve into ICMEs interacting with the solar wind and other CMEs. Most ICMEs tend to attain the speed of the background solar wind although the very fast ones continue to have high speeds at 1 AU and beyond. ICMEs are responsible for the intense geomagnetic storms and large solar energetic particle events. The interplanetary magnetic field enhances significantly during the passage of ICMEs, typically increasing higher by a factor of 4 above the background value at 1 AU. Many CMEs drive shocks and continue to do so at 1 AU. Typically more shocks (than ICMEs) are observed by spacecraft along the Sun-Earth line, because the shocks are more extended than the driving ICMEs. Ions with high charge are observed in ICMEs, especially those with magnetic cloud structure. These ions are indicative of the higher temperature in the source region near the Sun. Such high temperatures prevail in the flaring regions, generally located beneath the erupting CMEs. ICMEs have to originate

close to the disk center to have direct impact on Earth's magnetosphere. Most of the ICMEs originating close to the disk center seem to have flux rope structure. ICMEs that cannot be classified as magnetic clouds generally originate at larger central meridian distances than MCs. This suggests that all ICMEs may have cloud structure when viewed appropriately. During solar minimum, ICMEs have wide range of latitudes, but almost all ICMEs seem to be magnetic clouds. This may be due to the strong influence of the global dipolar field of the Sun, which forces the CMEs to move close to the ecliptic lane. Although the rate of magnetic clouds do not follow the CME rate as a function of the solar cycle, all ICMEs taken together have a rate that agrees with the solar cycle variation of white-light CMEs.

The current knowledge on ICMEs and their solar origin has been primarily obtained from two-point observations: near the Sun from coronagraphs near Earth using in-situ measurements. The coronagraphic observations give information on the mass distribution in CMEs. One has to use non-coronagraphic observations such as in EUV and X-rays to get additional information such as temperature. On the other hand *in situ* observations provide a lot more information, but only along the trajectory of the observing spacecraft through the ICME. Radio observations at long wavelengths and interplanetary scintillation observations are the only way to get information on CMEs throughout the inner heliosphere, but they provide information on the shocked plasma ahead of CMEs. Future observations from the Heliospheric Imager on board the STEREO observations will enable direct comparison of CMEs and ICMEs using Thomson scattering technique. One of the major hindrances to the understanding of CMEs is the lack of direct observation of magnetic properties of CMEs near the Sun. Most investigations use magnetograms to get information on the CME magnetic field. Microwave and infrared techniques show some promise, but they need further development before routine information becomes available.

Acknowledgements

References

Aguilar-Rodriguez, E., Blanco-Cano, X., and Gopalswamy, N.: 2004, *Adv. Space Res.* **38**(3), 522.
Balogh, A.: 2002, *ASP Conf. Ser.* **269**, 37.
Balogh, A., Gosling, J. T., Jokipii, J. R., Kallenbach, R., and Kunow, H. (eds.): 1999, *Space Sci. Rev.* **89**, 1.
Borrini, G., Gosling, J. T., Bame, S. J., and Feldman, W. C.: 1982, *J. Geophys. Res.* **87**, 7370.

Bothmer, V., and Schwenn, R.: 1994, *Space Sci. Rev.* **70**, 215.

Bothmer, V., and Schwenn, R.: 1998, *Ann. Geophys.* **16**, 1.

Bravo, S., and Blanco-Cano, X.: 1998, *Ann. Geophys.* **16**, 359.

Burlaga, L. F.: 1995, *Interplanetary Magnetohydrodynamics*, Oxford University Press.

Burlaga, L., Sittler, E., Mariani, F., and Schwenn, R.: 1981, *J. Geophys. Res.* **86**, 6673.

Burlaga, L. F.: 1982, *Geophys. Res. Lett.* **9**, 1317.

Burlaga, L. F., Lepping, R. P., and Jones, J. A.: 1990, *Geophys. Monogr. Ser.* **58**, 373.

Burlaga, L. F., Behannon, K. W., and Klein, L. W.: 1987, *J. Geophys. Res.* **92**, 5725.

Burlaga, L. F., *et al.*: 1998, *J. Geophys. Res.* **103**, 227.

Burlaga, L. F., Plunkett, S. P., and St. Cyr, O. C.: 2002, *J. Geophys. Res.* **107**, A10, 1266, doi:10.1029/2001JA000255.

Cane, H. V., and Richardson, I. G.: 2003, *J.Geophys. Res. A* **108**, 6.

Chen, J., *et al.*: 1997, *Astrophys. J.* **490**, L191.

Chao, J. K., and Lepping, R. L.: 1974, *J. Geophys. Res.* **79**, 1799.

Cliver, E. W., Ling, A. G., and Richardson, I. G. : 2003, *Astrophys. J.* **592**, 574.

Dryer, M.: 1994, *Space Sci. Rev.* **67**, 363.

Galvin, A. B.: 1997, in N. Crooker, J. A. Joselyn, and J. Feynman (eds.), *Coronal Mass Ejections*, AGU, Washington D.C., 253.

Gonzalez, W. D., Chía de Gonzalez, A. L., Dal Lago, A., Tsurutani, B. T., Arballo, J. K., Lakhina, G. K., *et al.*: 1998, *Geophys. Res. Lett.* **25**, 963.

Gopalswamy, N.: 2002, *COSPAR Colloq. Ser.* **14**, 157.

Gopalswamy, N.: 2003, *Adv. Space Res.* **31**, 869.

Gopalswamy, N.: 2004, in G. Poletto and S. T. Suess (eds.), *The Sun and the Heliosphere as an Integrated System*, Kluwer, Boston, p. 201.

Gopalswamy, N.: 2006, *J. Astrophys. Astron.* **27**, 243.

Gopalswamy, N., Hanaoka, Y., Kosugi, T., Lepping, R. P., Steinberg, J. T., Plunkett, S., *et al.*: 1998, *Geophys. Res. Lett.* **25**, 2485.

Gopalswamy, N., Lara, A., Lepping, R. P., Kaiser, M. L., Berdichevsky, D., and St. Cyr, O. C.: 2000, *Geophys. Res. Lett.* **27**, 145.

Gopalswamy, N., Lara, A., Kaiser, M. L., and Bougeret, J.-L.: 2001a, *J. Geophys. Res.* **106**, 25,261.

Gopalswamy, N., Lara, A., Yashiro, S., Kaiser, M. L., and Howard, R. A.: 2001b, *J. Geophys. Res.* **106**, 29,207.

Gopalswamy, N., Yashiro, S., Kaiser, M. L., Howard, R. A., and Bougeret, J.-L.: 2001c, *Astrophys. J.* **548**, L91.

Gopalswamy, N., Shimojo, M., Lu, W., Yashiro, S., Shibasaki, K., and Howard, R. A.: 2003a, *Astrophys. J.* **586**, 562.

Gopalswamy, N., Yashiro, S., Lara, A., Kaiser, M. L., Thompson, B. J., Gallagher, P. T., *et al.*: 2003b, *Geophys. Res. Lett.* **30**, CiteID 8015.

Gopalswamy, N., Yashiro, S., Michalek, G., Xie, H., Lepping, R. P., and R. A.: 2005a, *Geophys. Res. Lett.* **32**, 12.

Gopalswamy, N., Lara, A., Manoharan, P. K., and Howard, R. A.: 2005b, *Adv. Space Res.* **36**, 2289.

Gopalswamy, N., Yashiro, S., Liu, Y., Michalek, G., Vourlidas, A., Kaiser, M. L., *et al.*: 2005c, *J. Geophys. Res.* **110**, 9.

Gopalswamy, N., Fleck, B., and Gurman, J. B.: 2005d, in *Proc. Asia Pacific Regional Conference of IAA*, Bangalore, India.

Gopalswamy, N., Akiyama, S., Yashiro, S., Michalek, G., Xie, H., Petty, S., *et al.*: 2006, *J. Atmos. Sol. Terr. Phys.*, submitted.

Gosling, J. T.: 1990, *Geophys. Monogr. Ser.* **58**, 343.

Gosling, J. T.: 1997, in N. Crooker, J. A. Joselyn, and J. Feynman (eds.), *Coronal Mass Ejections*, AGU, Washington D.C., 9.

Gosling, J. T.: 1996, *Ann. Rev. Astron. Astrophys.* **34**, 35.

Gosling, J. T., McComas, D. J., Phillips, J. L., and Bame, S. J.: 1991, *J. Geophys. Res.* **96**, 731.

Henke, T., *et al.*: 1998, *Geophys. Res. Lett.* **25**, 3465.

Henke, T., Woch, J., Schwenn, R., Mall, U., Gloeckler, G., von Steiger, R., *et al.*: 2001, *J. Geophys. Res.* **106**, 10,597.

Hirshberg, J., Bame, S. J., and Robbins, D. E.: 1972, *Sol. Phys.* **23**, 467.

Hori, K., and Culhane, J. L.: 2002, *Astron. Astrophys.* **382**, 666.

Howard, R. A., Michels, D. J., Sheeley, Jr. N. R., and Koomen, M. J.: 1982, *Astrophys. J.* **263**, L101.

Hundhausen, A. J.: 1997, in N. Crooker, J. A. Joselyn, and J. Feynman (eds.), *Coronal Mass Ejections*, AGU, Washington D.C., 1.

Hundhausen, A. J., Gilbert, H. E., and Bame, S. J.: 1968, *Astrophys. J.* **157**, L3.

Klein, L. W., and Burlaga, L. F: 1982, *J. Geophys. Res.* **87**, 613.

Kunow, H., Crooker, N., Linker, J., Schwenn, R., and von Steiger, R. (eds.): 2006, *Space Sci. Rev.* **123**, 1, doi:10.1007/s11214-006-9007-z.

Lepping, R. P., Burlaga, L. F., and Jones, J. A.: 1990, *J. Geophys. Res.* **95**, 11957.

Lepping, R. P., Wu, C.-C., and Berdichevsky, D. B.: 2005, *Ann. Geophys.* **23**, 2687.

Lepri, S. T., Zurbuchen, T. H., Fisk, L. A., Richardson, I. G., Cane, H. V., and Gloeckler, G.: 2001, *J. Geophys. Res.* **106**, 29,23,2001.

Lepri, S. T., and Zurbuchen, T. H.: 2004, *J. Geophys. Res.* **109**, A01112.

Lindsay, G. M., Russell, C. T., Luhmann, J. G., and Gazis, P.: 1994, *J. Geophys. Res.* **99**, 11.

Lindsay, G. M., Luhmann, J. G., Russell, C. T., and Gosling, J. T.: 1999, *J. Geophys. Res.* **104**, 12,515.

Low, B. C.: 1996, *Sol. Phys.* **167**, 217.

Manoharan, P. K., Gopalswamy, N., Yashiro, S., Lara, A., Michalek, G., and Howard, R. A.: 2004, *J. Geophys. Res.* **109**, 6109.

Marsden, R. G., Sanderson, T. R., Tranquille, C., Wenzel, K.-P., and Smith, E. J.: 1987, *J. Geophys. Res.* **92**, 11,009.

Martens, P. C. H., and Kuin, N. P. M.: 1989, *Sol. Phys.* **122**, 263.

Marubashi, K.: 1986, *Adv. Space Res.* **6**, 335.

Mulligan, T., Russell, C. T., Elliott, D., Gosling, J. T., and Luhmann, J. G.: 2001, *Geophys. Res. Lett.* **28**, 891.

Munro, R. H., Gosling, J. T., Hildner, E., MacQueen, R. M., Poland, A. I., and Ross, C. L.: 1979, *Sol. Phys.* **61**, 201.

Neugebauer, M., and Goldstein, R.: 1997, in N. Crooker, J. A. Joselyn, and J. Feynman (eds.), *Coronal Mass Ejections*, AGU, Washington D.C., 245.

Parker, E. N.: 1957, *Astrophys. J. Supp.* **3**, 51.

Pevtsov, A. A., Canfield, R. C., and Latushko, S. M.: 2001, *Astrophys. J.* **549**, L261.

Pinter, S.: 1973, *Nature Phys. Sci.* **243**, 96.

Rao, U. R., McCracken, K. G., and Bukata, R. P.: 1967, *J. Geophys. Res.* **72**, 4325.

Reinard, A.: 2005, *Astrophys. J.* **620**, 501.

Riley, P., Schatzman, C., Cane, H. V., Richardson, I., and Gopalswamy, N.: 2006, in press.

Roussev, I. I., and Sokolov, I. V.: 2006, *Geophys. Monogr. Ser.* **162**, in press.

Russell, C. T., and Shinde, A. A.: 2005, *Sol. Phys.* **229**, 323.

Rust, D. M.: 1999, *Geophys. Monogr. Ser.* **111**, 221.

Schwenn, R., dal Lago, A., Huttunen, E., and Gonzalez, W. D.: 2005, *Ann. Geophys.* **23**, 625.

Sheeley, N. R., Howard, R. A., Koomen, M. J., Michels, D. J., Schwenn, R., Muhlhauser, K.-H., *et al.*: 1985, *J. Geophys. Res.* **90**, 163.

Sonnet, C. P., Colburn, D. S., Davis, L., Smith, E. J., and Coleman, P. J.: 1964, *Phys. Rev. Lett.* **13**, 153.

Srivastava, N., and Venkatakrishnan, P.: 2004, *J.Geophys. Res. A* **109**, 10103.

Tousey, R.: 1973, *Space Res.* **13**, 713.

Tsurutani, B. T., and Gonzalez, W. D.: 1997, *Geophys. Monogr. Ser.* **98**, 77.

von Steiger, R., Geiss, J., Gloeckler, G., and Galvin, A. B.: 1995, *Space Sci. Rev.* **72**, 71.

von Steiger, R., and Zurbuchen, T.: 2003, in *Proc. International Solar Cycle Studies (ISCS) Symposium*, Vol. 535 of *ESA SP*, p. 835.

Wang, Y. M., Ye, P. Z., Wang, S., Zhou, G. P., and Wang, J. X.: 2002, *J. Geophys. Res.* **107**, 1340, doi:10.1029/2002JA009244.

Webb, D. F., Cliver, E. W., Crooker, N. U., St. Cry, O. C., and Thompson, B. J.: 2000, *J. Geophys. Res.* **105**, 7491.

Wilson, R. M., and Hildner, E.: 1986, *J. Geophys. Res.* **91**, 5867.

Wu, Chin-Chun, Lepping, R. P., and Gopalswamy, N.: 2003, in *Proc. International Solar Cycle Studies (ISCS) Symposium*, Vol. 535 of *ESA SP*, p. 429.

Wu, Chin-Chun, Lepping, R. P., and Gopalswamy, N.: 2006, *Sol. Phys.*, in press.

Xie, H., Gopalswamy, N., Manoharan, P. K., Lara, A., Yashiro, S., and Lepri, S.: 2006, *J. Geophys. Res.* **111**, A01103.

Yurchyshyn, V., Wang, H., Goode, P. R., and Deng, Y.: 2001, *Astrophys. J.* **563**, 381.

Zhang, G., and Burlaga, L. F.: 1988, *J. Geophys. Res.* **93**, 2511.

Zhang, J., Dere, K. P., Howard, R. A., and Bothmer, V.: 2003, *Astrophys. J.* **6582**, 520.

Zwickl, R. D., Asbridge, J. R., Bame, S. J., Feldman, W. C., and Gosling, J. T.: 1982, *J. Geophys. Res.* **87**, 7379.